Contrib Mineral Petrol (1989) 101:207–219

Contributions to Mineralogy and Petrology

Petrology and U/Pb geochronology of the Telohat migmatites, Aleksod, Central Hoggar, Algeria *

Pierre Barbey [1,2], **Jean-Michel Bertrand** [2], **Serge Angoua** [1,2], **and Danielle Dautel** [2]

[1] Laboratoire de Pétrologie, Université de Nancy I, B.P.239, F-54506 Vandoeuvre-lès-Nancy cedex, France
[2] Centre de Recherches Pétrographiques et Géochimiques, B.P.20, F-54501 Vandoeuvre-lès-Nancy cedex, France

Abstract. The Aleksod region is composed of metasedimentary rocks and large areas of biotite and hornblende-bearing migmatites. Anatexis associated with the main deformation stages, occurred under high pressure and temperature conditions estimated at 13 ± 2 Kbar and $750 \pm 50°$ C. The bulk mineralogical composition of the Telohat migmatites shows that their protolith was granodioritic. Internal structures of zircons and U – Pb data suggest a polyphased evolution, with a 2131 ± 12 Ma age for the protolith and a 609 ± 17 Ma age for the Pan-African tectono-metamorphic evolution, thus precluding any Kibaran event in the Aleksod area. Leucosomes are richer in Sr and display lower Rb, Zr, Nb, Y, Th, U and REE contents than melanosomes wherein accessory phases are stored. Eu contents are also lower in the leucosomes but in lesser proportion than the other rare earth's, leading to a significant positive anomaly. Petrogenetic modelling accounting for accessory mineral phases clearly shows that the trace element contents of leucosomes and melanosomes follow a distribution law consistent neither with equilibrium nor fractional melting. Their trace element patterns are best explained by the model of disequilibrium melting, with mixing of a few residual phases. The present results and previous Sr isotopic data as well raise the question of disequilibrium melting in anatexis of crustal material

Introduction

The trace element behaviour during crustal anatexis is modelled assuming equilibrium melting conditions. Some studies have shown, however, that the distribution of trace elements in migmatites does not fit equilibrium distribution. This has been accounted for by several mechanisms, such as: (1) mixing between melts and refractory phases (Weber et al. 1985) or between locally derived melts and injected magmas (Weber and Barbey 1986); (2) fractional crystallization (Cuney and Barbey 1982; Sawyer 1987); or (3) disequilibrium melting (Pushkar and Stoeser 1975; Deniel 1985).

The Telohat migmatites (Aleksod area, Central Hoggar), previously considered to have formed during a 1.0 Ga Kibaran event (Bertrand 1974; Bertrand and Lasserre 1976), are an interesting case-study in this respect. The present study has two main purposes: (1) a reappraisal of the age of the migmatitic unit through zircon U/Pb chronology, as recent data preclude a Kibaran imprint in the neighbouring regions (Bertrand et al. 1986), and (2) determination of the petrogenesis of the migmatites by use of combined petrographical observations and major and trace element data.

Geological setting

The tectono-metamorphic evolution of the region (Fig. 1a) as first described by Bertrand (1974) and recently re-interpreted by Bertrand et al. (1986) can be summarized as follows:

(1) The oldest formation (the Arechchoum formation) consists of tonalitic grey gneisses and granitic orthogneisses with minor metasediments. Available Rb/Sr whole-rock isochron (Bertrand 1974; Bertrand and Lasserre 1976) and U/Pb dating on zircon from granulite-facies rocks of the Tamanrasset and Oumelalen areas (Latouche and Vidal 1974; Bertrand et al. 1986) have established the ca. 2.0 Ga age of the Arechchoum gneisses. However, part of these gneisses (especially tonalitic grey gneisses) may represent Archaean remnants as suggested by the ca. 3.4 Ga Pb/Pb ages reported by Latouche (1978).

(2) The Aleksod formation is separated from the Arechchoum gneisses by the Ouadenki unconformity, re-interpreted as a major deep-seated early thrust linked to the main Pan-African nappe-stacking event, 615 Ma ago (Bertrand et al. 1986). The formation consists of metasediments (quartzites, marbles and metapelites) and of large volumes of mafic rocks and biotite-hornblende-bearing migmatites, granodioritic in composition (the Telohat migmatites, subject of the present study; Fig. 1b). Poorly defined Rb/Sr isochron ages of ca. 1.0 Ga (Bertrand and Lasserre 1976) suggested that its tectono-metamorphic evolution represented a Kibaran event. However, the Aleksod metasediments may correspond to the 2.0 Ga formations in the Tamanrasset and Oumelalen areas (Latouche 1978), which they closely resemble in both lithology and structure. The postulate is supported by the new results presented in this paper.

(3) The youngest formation (Pharusian) occurs as the low-grade Arefsa schist belt. It has been recognized for a long time to represent Upper Proterozoic volcaniclastic rocks affected by the Pan-African orogeny (Lelubre 1952). This formation is separated from the high-grade gneisses by the Pharusian unconformity which now appears to be a major tectonic contact outlined by mylonites and sealed by syntectonic granites (M. Briedj, personal communication 1987).

Pan-African reworking processes are controlled by deep-seated thrust tectonics which was initiated under high-grade amphibolite-facies conditions and evolved continuously to low-grade conditions (Boullier and Bertrand 1981; Bertrand et al. 1986). Pre- to syntectonic granites, emplaced just before or during this event, were dated in the 630–600 Ma range (zircon U/Pb dating) with a younger

* CRPG Contribution no 782

Offprint requests to: P. Barbey

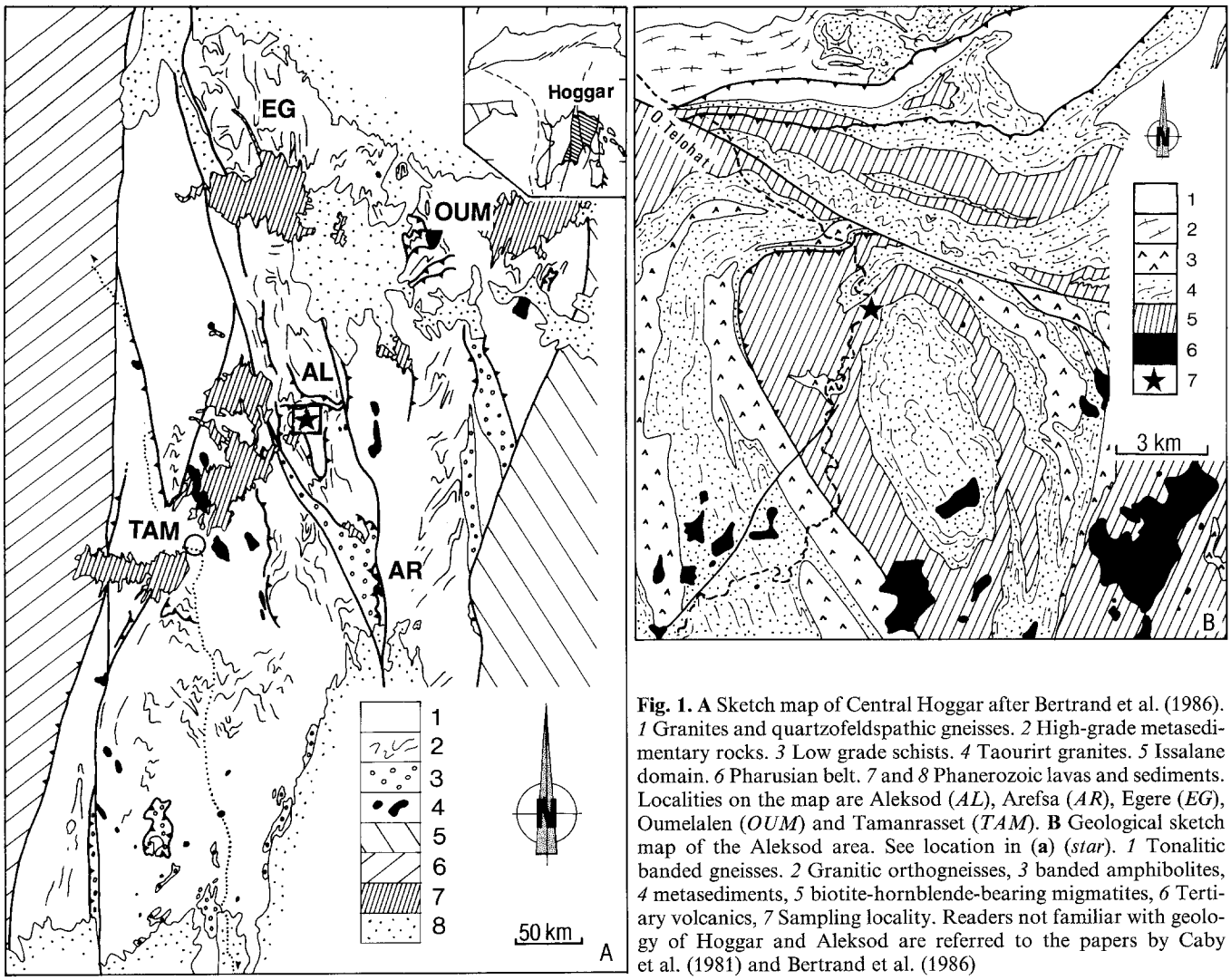

Fig. 1. A Sketch map of Central Hoggar after Bertrand et al. (1986). *1* Granites and quartzofeldspathic gneisses. *2* High-grade metasedimentary rocks. *3* Low grade schists. *4* Taourirt granites. *5* Issalane domain. *6* Pharusian belt. *7* and *8* Phanerozoic lavas and sediments. Localities on the map are Aleksod (*AL*), Arefsa (*AR*), Egere (*EG*), Oumelalen (*OUM*) and Tamanrasset (*TAM*). **B** Geological sketch map of the Aleksod area. See location in (**a**) (*star*). *1* Tonalitic banded gneisses. *2* Granitic orthogneisses, *3* banded amphibolites, *4* metasediments, *5* biotite-hornblende-bearing migmatites, *6* Tertiary volcanics, *7* Sampling locality. Readers not familiar with geology of Hoggar and Aleksod are referred to the papers by Caby et al. (1981) and Bertrand et al. (1986)

age (580 Ma) for the related sphenes and monazites (Bertrand et al. 1986).

Estimation of (P,T) conditions

The Pan-African tectono-metamorphic patterns of the Aleksod area result from a three stage evolution (Bertrand et al. 1986). The two first phases, corresponding to isoclinal recumbent folds followed by thrust tectonics, occurred under high-grade conditions and were accompanied with partial melting. The related mineral assemblages (symbols for mineral phases according to Kretz 1983) are as follows: (1) Qtz + Kfs + Pl + Hbl + Bt + Grt in biotite-hornblende gneisses and (2) Pl + Hbl + Grt + Qtz + Ilm + Bt in hornblende gneisses. The incipient breakdown of biotite into hornblende together with partial melting, in the granodioritic migmatites, suggests that temperatures of at least 700° C were reached (Kenah and Hollister 1983). Muscovite and kyanite are stable in the migmatitic metapelites; this implies, for anatexis, pressure conditions higher than 7 Kb (Fig. 2). The third tectono-metamorphic phase (late wrench-fault tectonics) occurred under retrograde conditions and is characterized by epidote, prehnite, green biotite and carbonate assemblages.

Mineral compositions were determined with an automatized CAMEBAX electron microprobe (University of Nancy I) operating at 15 kV, 10 nA and using ZAF correction procedures.

Temperatures were estimated from Grt – Bt assemblages in metapelites, using the calibration of Ferry and Spear (1978), Pigage

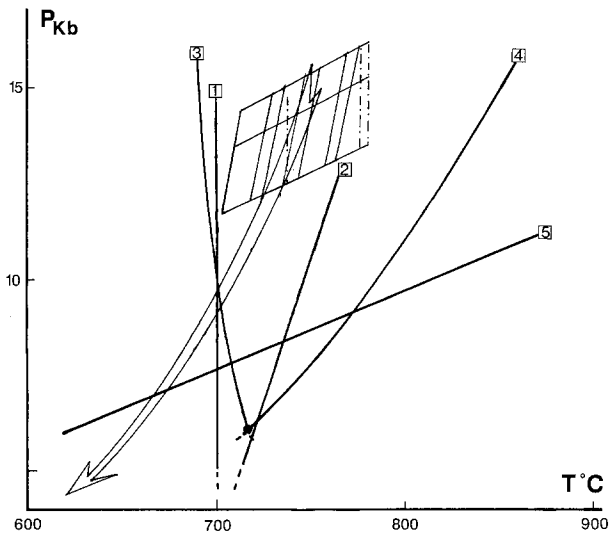

Fig. 2. P – T conditions for the studied area (*box*) determined from Bt – Grt – Pl – Ky – Qtz thermobarometry (*solid lines*) and Grt – Hbl thermometry (*dot-dashed lines*). *1* Bt + Pl + V = Hbl + L and *2* Bt + Pl = Hbl + Kfs + L from Kenah and Hollister (1983); *3* Ms + Or + Qtz + V = L and *4* Ms + Qtz = Or + Al – Sil + L from Thompson and Algor (1977); *Arrow*: P – T – t path for the Aleksod eclogites (Sautter 1986)

and Greenwood (1979) and Hodges and Spear (1982), and from Grt-Hbl assemblages in amphibolites, using the calibration of Powell (1985). The temperatures given by the calibration of Ferry and Spear (690–750° C) are intermediate between those obtained from the calibrations of Pigage and Greenwood (740–810° C) and Hodges and Spear (635–740° C); they are consistent with temperatures yielded by the Grt-Hbl thermometer (738–782° C). Pressures have been estimated from Grt−Pl−Ky−Qtz assemblages using the calibration of Newton and Haselton (1981) with the garnet solid solution model of Ganguly and Saxena (1984). Pressure estimates are between 11 and 15 Kbar for temperatures ranging from 700 to 750° C (Fig. 2), except for two lower values around 8 Kbar. The peak metamorphic conditions are estimated at roughly 750 ± 50° C and 13 ± 2 Kbar, in agreement with the P−T−t path reconstructed for the Aleksod eclogites (Sautter 1986). This rough estimate indicates that initial melting of granitic rocks could have occurred at $X_{H_2O} \geq 0.4$.

Petrography

The migmatites formed by partial melting of biotite-hornblende gneisses. They are mainly layered and nebulitic migmatites and, locally agmatitic when disrupted amphibolitic layers are present (migmatite nomenclature according to Dietrich and Mehnert 1960 and Johannes 1983). The study samples are of two types: one leucosome/melanosome/mesosome triplet (sample E-114) and three leucosome/melanosome pairs (samples G-131-133), such as shown in Fig. 3a and b respectively. Leucosomes and melanosomes are always closely associated and their proportions are rather constant: the mass fraction of leucosome/(leucosome+melanosome), estimated by image processing and respective densities ranges from 0.45 to 0.55. Textures are granoblastic in all parts of the migmatites.

Mesosome

Mesosomes are medium-grained (0.5–1 mm), dominantly biotite-hornblende layered gneisses with a weak but continuous foliation. The mineralogical compositional range in any layer is quartz (15–25 vol.%), K-feldspar (10–20%), plagioclase (40–60%), biotite, hornblende and garnet (15–25%). The mesosome studied (E-114) is composed of quartz (20%), K-feldspar (12%), plagioclase An_{30-40} (52%), biotite (12%), hornblende (3%), garnet (0.5%) and accessories (allanite, apatite, sphene and zircon); secondary phases are chlorite, epidote, prehnite and carbonate. A small amount of allanite, apatite, sphene and zircon are included in biotite and hornblende (~1 vol.% of the host mineral).

Leucosome

Leucosomes are medium to coarse-grained (0.5–5 mm), composed of quartz (25–30 vol.%), K-feldspar (25–35%) and plagioclase An_{20-35} (40–50%).

These quartzofeldspathic segregations frequently contain clusters (< 5 mm) of biotite flakes and hornblende porphyroblasts.

Melanosome

Melanosomes are medium-grained (~1 mm) and composed of quartz (20–25 vol.%), K-feldspar (5%), plagioclase An_{20-30} (50%), hornblende ($X_{Fe}=0.68$; 5–10%), biotite ($X_{Fe}=0.60$–0.65; 15–20%) and garnet (0.5%). Garnets ($X_{Fe}=0.52$, $X_{Mn}=0.09$. $X_{Mg}=0.06$ and $X_{Ca}=0.33$) occur as small crystals or relict grains in hornblende and plagioclase. The compositions of hornblende, biotite and garnet from leucosome and mesosome are the same as in melanosome. Retrograde phases are green biotite, epidote, prehnite and carbonate.

The most striking feature of the melanosomes is the high content of accessory minerals (apatite, allanite, sphene and zircon). Accessories are often included in the major ferromagnesian phases; the volume fraction of these inclusions with respect to the host mineral (biotite or hornblende) never exceeds 0.05. Apatite occurs as small euhedral crystals (0.2 mm) frequently included in hornblende. Allanite occurs as subhedral to euhedral metamict grains, larger and more irregular (0.2 mm on average but up to 6 mm) than apatite. Most of allanite crystals are surrounded by a rim of epidote or, more rarely, garnet. Others are large euhedral crystals overgrown on a metamict core. Sphene occurs as euhedral small (0.1–0.3 mm) grains or as long acicular grains located either along the cleavage or at the grain boundaries of biotite flakes. Zircons occur as light pink to light brown grains with complex zoning patterns described below.

Zircon U−Pb data

Zircon grains show rounded shapes or elongated bipyramids with rounded angles. Internal textures suggest a com-

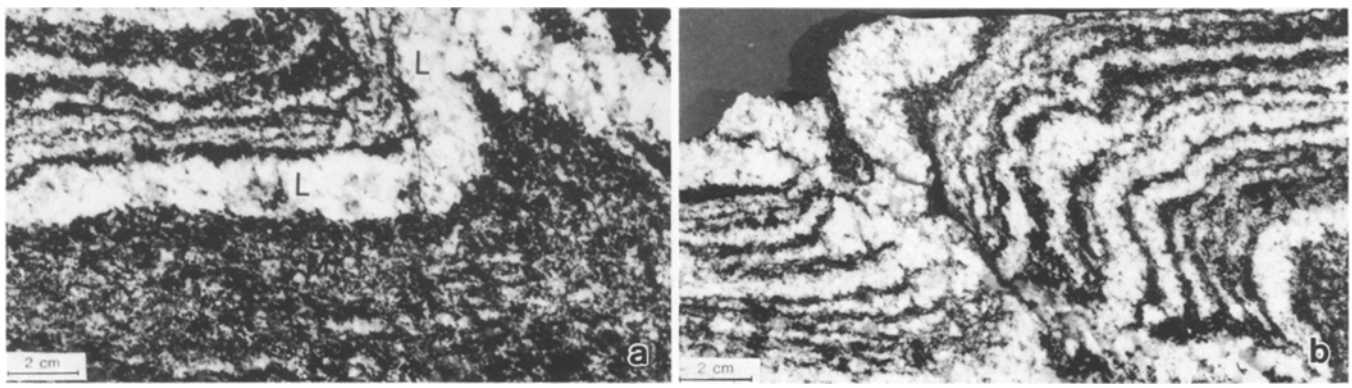

Fig. 3a, b. The biotite-hornblende migmatites. **a** Leucosome separated from a mesosome by a biotite-hornblende-rich melanosome; **b** Stromatic migmatites with alternate leucosomes and melanosomes; the quartzofeldspathic segregations tend to coalesce in the fold hinge

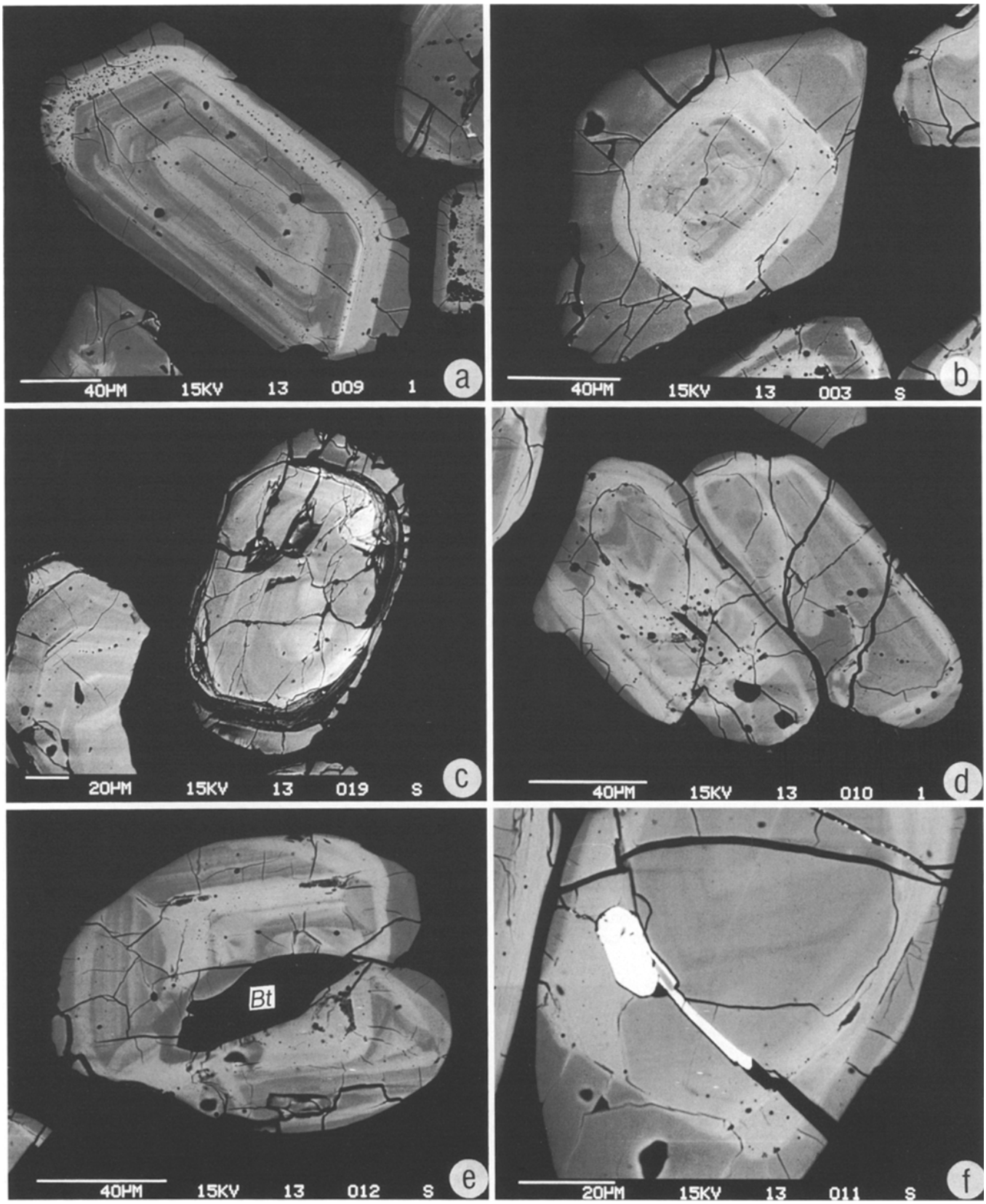

Fig. 4a–f. Back-scattered electron SEM photomicrographs of zoning patterns of zircons. **a** Zircon grain with zoned euhedral core surrounded by an intermediate rim (light grey) containing numerous tiny inclusions and by an outer rim forming a facetted shell; **b** Zircon with a zoned euhedral core showing resorption embayement related to the growth of the intermediate rim (light grey); **c** Polished zircon grain etched by HF, showing the U-rich intermediate rim (black); **d** Composite zircon formed of two crystals sealed by the outer rim; **e** Outer rim around a biotite crystal cross-cutting the intermediate light rim; **f** Late monazite within a fracture

Table 1. U–Pb analytical data on zircon from the Telohat migmatites. Size of zircon fractions: $B = 150–100$ μm, $C = 100–75$ μm and $D = 75–45$ μm

Fraction	Pb	U	206Pb /204Pb	207Pb* /235U	206Pb* /238U	207Pb /206Pb*	Model ages 207Pb* 235U	206Pb* /238U	207Pb* 206Pb*
B	137.3	658	9590	3.2079	0.2094934	0.111060	1459	1226	1817
C(m)	179.7	791	10321	3.5767	0.2261029	0.114728	1544	1314	1876
C	149.1	601	12185	4.0052	0.2457523	0.118202	1635	1417	1929
D	156.6	603	12543	4.2300	0.2569169	0.119413	1680	1474	1948

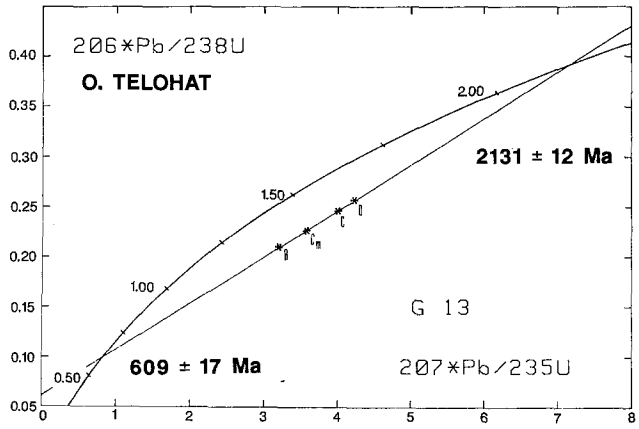

Fig. 5. Concordia plot for the U–Pb zircon data for the Telohat migmatites (see Table 3)

plex crystallization/recrystallisation history. In the simplest case, three distinctive zones may be observed:
- a zoned euhedral core (Fig. 4a, b) which is assumed to represent igneous zircon, showing resorption embayments (Fig. 4b) and containing large inclusions, some of which are polymineralic (e.g. quartz, biotite, pyroxene);
- an intermediate light-coloured rim with abundant tiny inclusions of quartz, apatite and K-feldspar (Fig. 4a, b); HF etching of polished grains reveals that this zone is richer in U (Fig. 4c);
- an outer rim of clear zircon forming a facetted shell.

More complex patterns have also been observed (Fig. 4d, e). Crystallization of monazite within a fracture (Fig. 4f) postdates the three zones defined above.

Crystallization of the rims and growth of monazite along fractures are likely to be related to the metamorphic evolution of the host rock. The origin and timing of the U-rich intermediate zone is more doubtful, but cross-cutting relationships with the igneous core, indicating resorption, suggests that this zone could be also of metamorphic origin.

U and Pb isotopic compositions were determined using a CAMECA mass-spectrometer. Detailed analytical procedures are found in Bertrand et al. (1986). The results (Table 1 and Fig. 5) show to major events:

(1) one at 2131 ± 12 Ma which can be interpreted either as the age of crystallization of the granodioritic protolith of the migmatite or as the age of a tectono-metamorphic event which occurred shortly after the crystallization, and

(2) a tectono-metamorphic event at 609 ± 17 Ma which must be that of the migmatization. The high discordance of the zircon fractions and their location in the middle part of the discordia line (Fig. 5) may be interpreted either as an episodic lead loss or as a mixing line between two components with distinct isotopic composition (see also Bertrand et al. 1986). The 610 Ma age is already known in the Tamanrasset region where a penetrative deformation and related metamorphic evolution range between 615 and 580 Ma (Bertrand et al. 1986).

The U–Pb zircon age of the Telohat migmatites and the good resolution of the two concordia intercepts preclude any metamorphic event between 2100 and 600 Ma, and consequently confirm the lack of a Kibaran event in that region.

Major and trace element geochemistry

Major and trace elements (including REE) were analysed by ICP at CRPG (Nancy). Sample preparation, analytical procedures and precisions are found in Weber and Barbey (1986). REE are normalized to chondrite following Jahn et al. (1980). Whole-rock analytical data are given in the Table 2.

The major element composition of leucosomes close to cotectic compositions in the normative Qtz–Ab–Or diagram (Fig. 6) suggests that they were partial melts. They have higher Sr and lower Rb contents compared to the melanosomes (Fig. 7c), leading to lower Rb/Sr ratios in the leucosomes (<0.26) than in the melanosomes (>0.35). The REE content is low and the patterns are of two types (Fig. 8): one characterized by moderately fractionated REE with $(La/Yb)_N$ ratios around 5 and positive Eu anomalies (samples G-131, G-132), the other with strongly fractionated REE ($(La/Yb)_N = 17$) and a negative Eu anomaly (sample E-114). The Th, REE and Zr contents of the leucosome sample E-114 higher than those of the other samples are likely to be due to a higher amount of zircon and allanite.

The melanosome compositions are characterized by high Al, Fe, Mg, Ca as well as Zr, Nb, Y, Th, U and REE (Table 2). Partial microprobe analyses of accessories show that La, Ce and Th are mainly located in allanite ($La_2O_3 = 2.5$ wt%, $Ce_2O_3 = 4.5\%$. $ThO_2 = 0.2–1.5\%$) whereas Y is contained mainly in sphene ($Y_2O_3 = 0.5–2.2\%$) and zircon ($\sim 0.5\%$). This shows that the trace element compositions of melanosomes are controlled by the ferromagnesian and accessory phases. The melanosomes have the highest REE contents of the three zones and all display similar patterns (Fig. 8). Eu is also more abundant

Table 2. Major (wt%) and trace (ppm) element analytical data for the Telohat migmatites. The recasted composition for the sources of samples E-114 and G-132 are compared to the mesosome and to the average granodiorite from de la Roche et al. (1980); see explanations in the text

	Leucosomes			Melanosomes				Mesosome	Recasted sources		Average Granodiorite
	E-114	G-131	G-132	E-114	G-131	G-132	G-133	E-114	E-114	G-132	8
SiO_2	71.05	72.89	73.00	60.46	59.13	61.42	62.26	64.32	65.75	67.21	68.94
Al_2O_3	16.06	14.92	14.54	17.41	16.80	16.83	16.04	15.83	16.73	15.68	15.15
FeO*	0.71	0.29	0.37	6.04	7.28	6.14	6.03	4.59	3.37	3.26	3.42
MnO	–	0.02	0.02	0.13	0.10	0.08	0.09	0.10	0.07	0.05	0.07
MgO	0.2	0.03	–	1.68	1.81	1.54	1.59	1.49	0.94	0.77	1.18
CaO	2.90	1.91	2.33	4.18	3.95	3.53	3.76	3.66	3.54	2.93	2.95
Na_2O	4.32	3.55	4.09	4.47	4.27	4.29	4.23	4.10	4.40	4.19	3.66
K_2O	3.69	5.68	3.61	2.38	3.10	3.15	2.62	3.09	3.03	3.38	2.99
TiO_2	0.07	–	–	0.74	0.75	0.64	0.66	0.60	0.41	0.32	0.43
P_2O_5	0.08	–	–	0.29	0.25	0.13	0.11	0.19	0.19	0.07	0.16
L.i.	0.95	0.90	0.81	1.64	1.26	1.49	1.19	1.34	1.30	1.15	1.02
Total	100.02	100.19	98.77	99.56	98.67	99.24	98.58	99.84	99.73	99.00	99.97
Rb	83	107	67	135	144	135	123	94	109	101	
Sr	425	402	387	361	348	374	348	530	393	380	
Zr	75	46	57	274	230	195	263	274	175	126	
Nb	2	2	2	17	15	11	14	13	9	7	
Y	4	2	2	51	50	47	79	40	28	25	
Th	1.9	0.04	0.20	11.88	17.94	14.70	18.5	7.00	6.89	7.45	
U	0.5	0.49	0.41	1.98	2.88	1.97	2.58	0.98	1.24	1.19	
La	6.67	0.79	1.43	55.32	59.05	54.32	64.50	31.71	30.99	27.88	
Ce	18.76	2.78	4.11	120.77	135.55	119.60	153.35	75.31	69.77	61.85	
Nd	8.64	0.82	1.49	57.85	64.18	57.94	83.99	39.00	33.24	29.72	
Sm	1.96	0.18	0.27	12.31	13.09	12.12	19.76	8.05	7.13	6.19	
Eu	0.40	0.29	0.26	1.59	1.55	1.43	1.77	1.40	1.00	0.85	
Gd	1.33	0.17	0.27	11.92	10.18	9.49	15.77	6.88	6.63	4.88	
Dy	0.85	0.19	0.28	9.79	8.39	7.74	13.77	6.74	5.32	4.01	
Er	0.32	0.11	0.17	5.42	4.19	3.87	6.38	3.25	2.87	2.02	
Yb	0.25	0.12	0.17	5.19	3.97	3.75	5.67	2.95	2.72	1.96	
Lu	0.03	0.01	0.02	0.77	0.61	0.53	0.80	0.34	0.40	0.28	
Rb/Sr	0.20	0.26	0.17	0.37	0.41	0.36	0.35	0.18	0.28	0.26	
(La/Yb)N	17.00	4.47	5.68	7.03	10.04	9.78	7.68	7.09	7.52	9.31	
(La/Sm)N	2.05	2.77	3.34	2.74	2.84	2.82	2.06	2.40	2.65	2.75	
(Gd/Yb)N	4.18	1.15	1.28	1.84	2.07	2.05	2.25	1.87	1.96	1.98	
Eu/Eu*	0.48	4.99	2.92	0.40	0.40	0.39	0.29	0.56	0.44	0.46	

– Below detection limit

in the melanosomes than in the leucosomes, but in lesser amount than the other REE, leading to significant negative Eu anomalies (Eu/Eu* = 0.29–0.40).

The bulk composition of the mesosomes is granodioritic (Table 2 and Fig. 7), with a moderately fractionated REE pattern (Fig. 8), intermediate between leucosomes and melanosomes. Nevertheless, it is clear that the composition of this mesosome does not strictly correspond to that of the parent rock of the neosomes, due to low Al_2O_3 and Na_2O and high Sr and Zr contents. Such discrepancies between the neosome and mesosome major-element compositions have been reported on several occasions (Johannes and Gupta 1982; Gupta and Johannes 1986). The composition of the source will be discussed below, in more detail.

Petrogenetic modelling

The trace element composition of the Telohat migmatites has been modelled for Zr, REE, Rb and Sr.

The estimated P, T conditions and the near-cotectic composition of the leucosomes suggest melting of the Qtz–Kfs–Pl fraction. As indicated by petrographical data and by the low Rb contents of the leucosomes, incongruent melting of biotite remained minor and will not be considered here.

Accessory minerals and trace element modelling

In trace element modelling, the distribution coefficients for trace elements are based on the assumption that the trace elements obey Henry's law in the phases of interest. However, some accessory phases may contain the so-called "trace elements" as major components. Therefore, the Henry's law applies no longer and the melting equations (e.g. Shaw 1970) cannot be used (Montel 1987). Consequently, we have to distinguish between (Montel 1987):

(1) accessories rich in a trace element (such as zircon with REE) for which the melting equations and relevant partition coefficients may be used, and

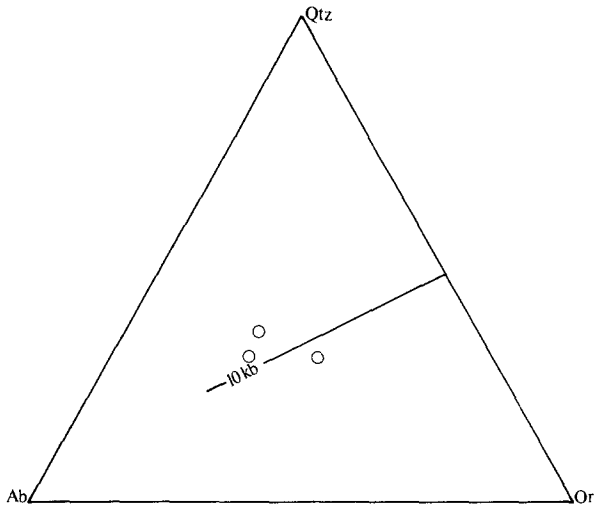

Fig. 6. Normative Qtz–Ab–Or diagram showing the position of the three analyzed leucosomes with respect to the cotectic line at $P_{H_2O}=10$ Kbar (Winkler 1978)

(2) accessories containing a trace element as a major component (such as zircon with Zr or apatite with P) whose partitioning into the melt is dependent on the solubility product but not on the degree of melting, therefore precluding the use of Shaw's equations.

Zr and REE

In the migmatites studied, Zr is controlled by zircon. Since the experimental work of Watson and Harrison (1983), the

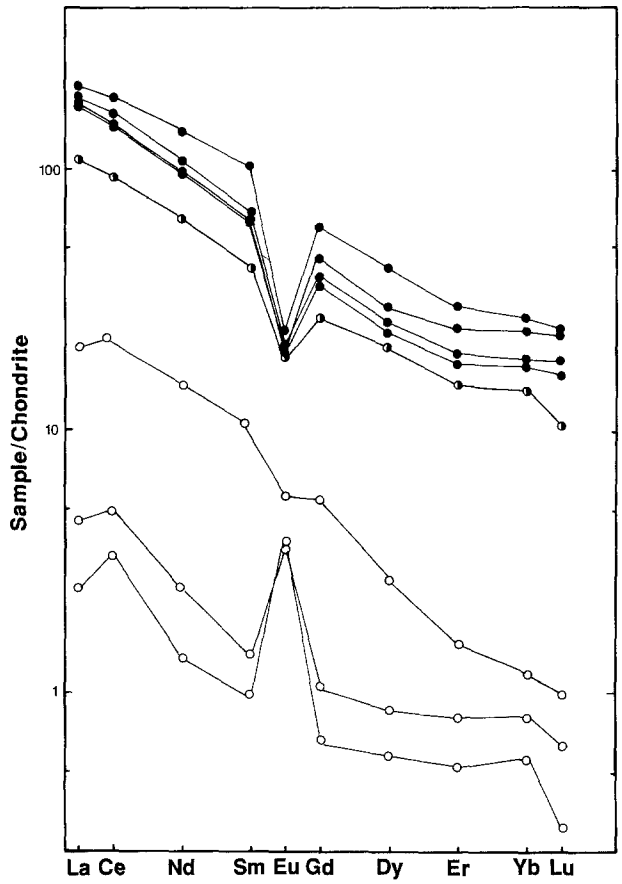

Fig. 8. Chondrite-normalized REE patterns for the leucosomes (*open circles*), melanosomes (*solid circles*) and mesosome (*half-filled circle*)

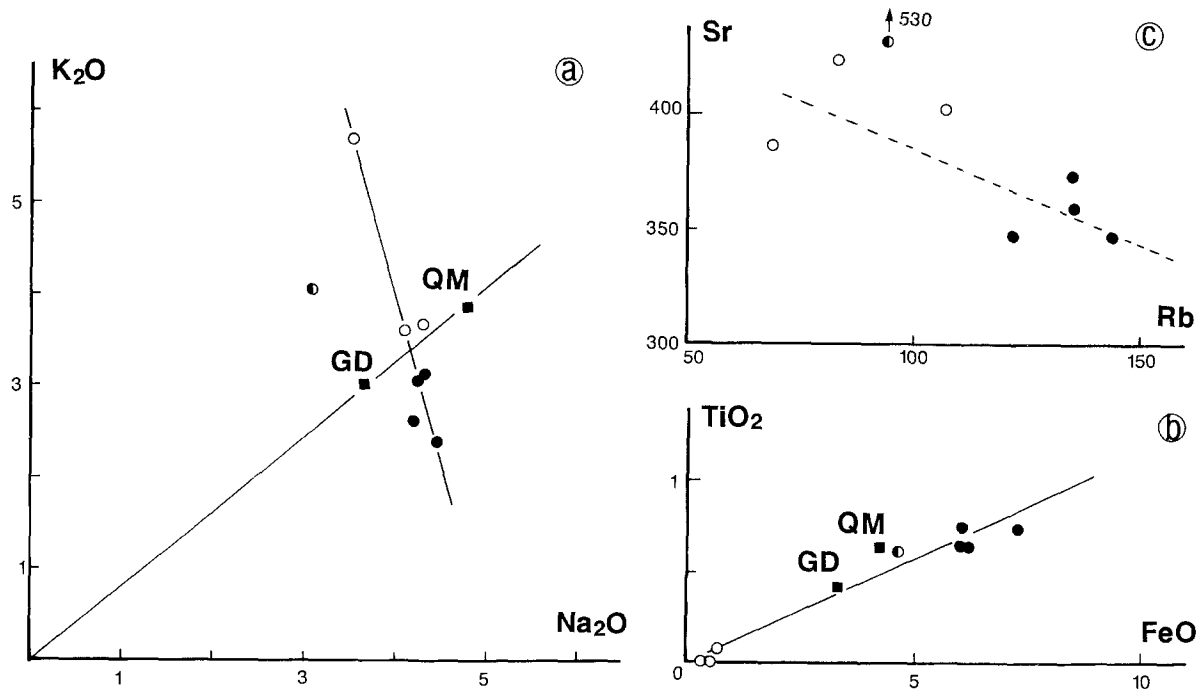

Fig. 7. a K_2O-Na_2O, **b** TiO_2-FeO and **c** Rb–Sr variation diagrams for the leucosomes (*open circles*), melanosomes (*solid circles*) and mesosome (*half-filled circle*). Average granodiorite and quartz-monzonite from de la Roche et al. (1980)

Table 3. Mineral compositions (wt%) of the source rocks and melts used for trace element modelling

	Qtz	Kfs	Pl	Bt	Hbl	Grt	Zrn	Ap	All	Sph
Source rocks:										
mesosome (E-114)	19	11	50	15	4	0.3	0.05	0.3	0.3	0.05
recasted composition (G-132)	22.3	15	48	10	4	0.3	0.02	0.1	0.25	0.05
Melts:										
equilibrium/fractional melting	29.95	30	40	0	0	0	0.02	0.025	0	0
disequilibrium melting	30	30	40	0	0	0	0	0	0	0

temperature effect upon solubilities of zircon in per- and metaluminous silica-rich melts ($SiO_2 \sim 73\%$) is known and the amount of dissolved zircon can be determined. Using the equation given by Watson (1987; appendix), and assuming temperatures of 720–750° C, the equilibrium amounts of Zr in the melt are estimated at 65–95 ppm. The Zr contents of leucosomes G-131/132 (46 and 57 ppm) are significantly lower than the predicted values, suggesting that saturation has not been reached and consequently that partial melting may have occurred under non-equilibrium conditions.

The REE contents of major mineral phases as well as zircon, apatite and sphene are low enough to allow the use of Shaw's equations (Shaw 1970) in modelling their distribution between a melt and a crystalline residue. More difficult is the case of allanite: as it may contain several weight percents LREE, its solubility product will largely control their partition during partial melting. Unfortunately, there is no data on allanite solubility in granitic melts. Nevertheless, as the LREE content of allanite in melanosomes is not very high, we have assumed that REE obey Henry's law and can be modelled with classical melting equations and relevant partition coefficients for rhyolitic melts (see appendix).

Composition of the source rock

The complete melting under water-saturated conditions, of the K-feldspar component of the gneisses leads to a degree of melting of 0.5, a value consistent with the estimated mass fraction of leucosomes and melanosomes. Melting under water-undersaturated conditions will increase the orthose component into the melt (Steiner et al. 1975; Pichavant 1987; Holtz et al. 1988) and, therefore, lower the degree of melting estimated. Consequently, it can be assumed that no significant melt removal occurred. Thus, the composition of the source rock can be roughly estimated from the leucosome and melanosome compositions and their mass fractions. As recasted, the compositions of the parent rock are close to that of granodiorites (Table 2) and not far from the mesosome composition, except for Sr and Zr. Modelling has been performed using both the mesosome and the recasted parent rocks as sources for the melts. The mineral proportions (Table 3) have been estimated from modal data and major and trace element compositions of both whole rocks and minerals.

Melting models

Three models can be reasonably considered and will be discussed: (1) equilibrium melting which is frequently used for trace element modelling during anatexis, (2) fractional melting in which the melts are assumed to be continuously removed and aggregated to form a leucosome, and (3) disequilibrium melting when trace element partitioning between minerals and melt failed to attain equilibrium (Allègre and Minster 1978). The relevant equations and partition coefficients are given in appendix. The calculation procedure is as follows.

The leucosome average major element composition is assumed to be representative of the melt composition. The proportions of quartz, K-feldspar and plagioclase component in the melt (Table 3) have been estimated from major element compositions of both whole rock and minerals.

For equilibrium and fractional melting models, the amounts of zircon and apatite dissolved into the melt (Table 3) were estimated from Watson's equations (1987). They correspond, on average, to 0.020 wt% and 0.025 wt% dissolved zircon and apatite, respectively (see appendix). The amounts of dissolved allanite and sphene as well as the amounts of entrained accessories cannot be determined and have been assumed to be zero. Consequently, the equilibrium and fractional melt REE contents are minimum estimates. The calculations have been performed for $0.1 \leq F \leq 0.5$.

In disequilibrium melting, the concentration of an element in the melt depends both on its concentration in the mineral phases and on the weight proportion of minerals contributing to the melt (see appendix). As we are out of equilibrium, the amount of accessory minerals dissolved into the melt cannot be estimated as it depends on several parameters (such as the amount of accessories hosted in the major refractory phases). Further, as minerals entrained into the melt (mixing) have the same effect upon trace element distribution, the amount of minerals entrained cannot be estimated. Consequently, we have modelled the melt compositions in two stages:

(1) we have assumed that only quartz, K-feldspar and plagioclase contribute to the melt, in the proportions given by the leucosome average composition (Table 3);

(2) then we have examined the effect of dissolution (or mixing) of major ferromagnesian phases (hornblende + biotite) and accessory phases.

Discussion

Equilibrium and fractional melting

The model REE contents of partial melts obtained assuming either equilibrium melting or fractional melting, for $0.1 \leq F \leq 0.5$, are in a restricted range (Fig. 9a dashed area).

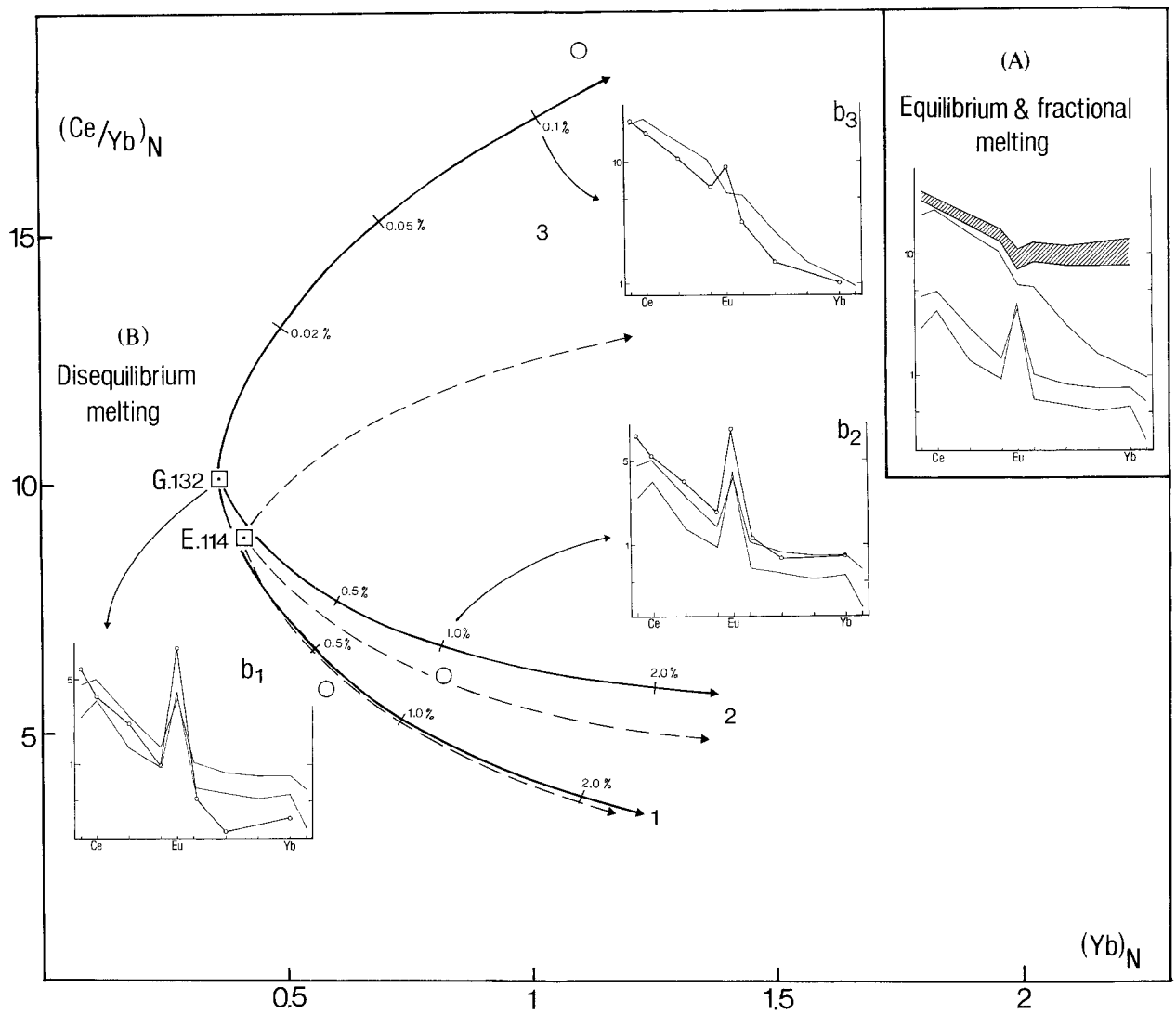

Fig. 9A, B. Diagrams showing the results of REE modelling. **A** Equilibrium and fractional melting. REE compositional range for melts (*hatched area*) arising from partial melting ($0.1 < F < 0.5$) of the mesosome E-114 and the recasted source G-132 (Table 2); leucosomes are shown for comparison (*light lines*). **B** Disequilibrium melting. $(Ce/Yb)_N$ vs $(Yb)_N$ diagram showing the model melt compositions obtained assuming disequilibrium melting of the same sources (*dotted squares* and *diagram b1*), and the effect of mixing (or dissolution) of refractory phases: Trends (1) – mixing of biotite and hornblende in the same ratio as in the source; Trends (2) – mixing of biotite and hornblende (in the same ratios as in the source) containing 1% of accessory inclusions; the melt composition, produced when 1 wt% mafic minerals is mixed into the melt, is compared to the leucosomes G-131/132 (*diagram b2*); Trends (3) – mixing of accessories in the same ratio as in the source; the melt composition produced by mixing 0.1 wt% accessories into the melt is compared to the leucosome E-114 (*diagram b3*)

The melt LREE or HREE contents, given by both models, differ markedly from those of the leucosomes, at least by one order of magnitude as they are minimum estimates.

As it appears on Rb/Sr binary plots (Fig. 10), equilibrium melting should lead to melts characterized by Rb/Sr ratios significantly higher (>0.50) than those of the related residues (<0.25). The same patterns are obtained assuming fractional melting. Therefore, the REE, Rb and Sr patterns of the leucosomes cannot only be accounted for by equilibrium or fractional melting models.

The role of fluids

As partial melting in migmatites involves volatile components, the leucosome trace element patterns may be regarded as later features due to element fractionation with a fluid phase. Two cases must be considered:

(1) The fluid exsolved from the melt during crystallization. Experimental studies on Rb and Sr (Carron and Lagache 1980) or REE (Flynn and Burnham 1978) fractionation between rhyolitic melts and aqueous fluid at 800° C clearly show that the melt/fluid partition coefficients are >1. Consequently, the removal of a fluid phase from the melt, during crystallization, will lead to leucosomes enriched in Rb, Sr and REE with respect to modelled equilibrium melt compositions. This is at variance with the leucosome compositions observed (Figs. 9 and 10).

(2) An externally derived fluid percolated through the migmatite. As the concentration in REE of hydrothermal solutions is very low (e.g. Michard and Albarède 1986) and

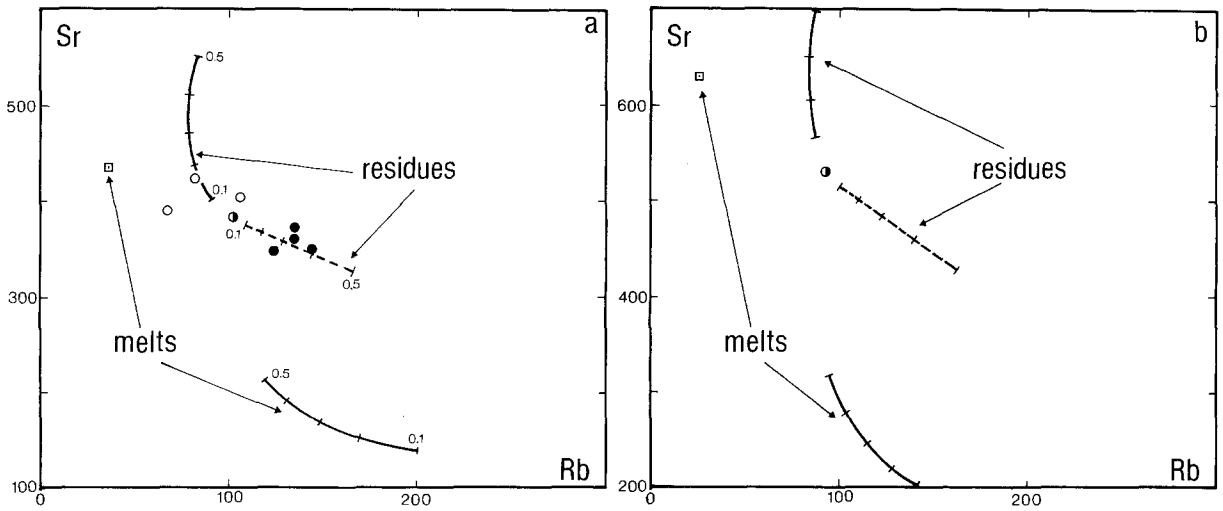

Fig. 10a, b. Sr–Rb diagrams for modelled melts and residues and the related parent rocks (*half-filled circle*) assuming either equilibrium melting (*heavy lines*) or disequilibrium melting (*dashed line* and *dotted square*). Numbers on the curves refer to the degree of melting. Note the inversion of the relative position of melt and residue between disequilibrium and equilibrium melting. **a** Model using the recasted composition G132 (Table 2) as the source: leucosomes (*open circles*) and melanosomes (solid circles) shown for comparison; **b** Model using the mesosome E114 (Table 2) as the source

as the bulk of the REE is hosted in the accessory phases, such a process would require high water/rock ratio and the dissolution or reequilibration of accessories. This appears unlikely because accessories from leucosomes, melanosomes and mesosomes are identical in both morphology and composition and because the percolation of a fluid phase will tend to homogeneize the whole migmatite.

The chemical patterns of leucocomes are, therefore, believed to be primary features. The distribution of the trace elements in these rocks can be considered to result (1) from a lit-par-lit transformation of layered gneisses, (2) from a lit-par-lit injection, (3) from subsolidus differentiation followed by partial melting, (4) from disequilibrium melting.

Lit-par-lit transformation or injection do not appear likely as main processes (even though melting may occurred under open system conditions), as they account neither for the differentiation of melanosome segregations nor for the rather constant proportions of leucosome to melanosome, around 0.5. As the leucosomes and mesosomes are characterized by the same mineral assemblage, there would have been no significant chemical gradient between melts and the surrounding rocks. Therefore, the melanosomes are unlikely to be reaction zones.

Disequilibrium melting

The modelled LREE contents obtained assuming disequilibrium melting (Fig. 9B) are close to the composition of leucosomes. The best approximation is obtained assuming mixing (±dissolution) of a small amount of residual phases: either biotite and hornblende containing accessory inclusions, for samples G-131/132 (Figs. 9, b2), or accessories for sample E-114 (Figs. 9, b3).

The melt compositions resulting from disequilibrium melting display lower Rb/Sr ratios (0.10) than the related residues (>0.30), consistent with the compositions of leucosomes and melanosomes of the migmatites studied (Fig. 10). The distribution of both Rb and Sr in these migmatites are therefore also consistent with the disequilibrium melting model.

However, as both subsolidus differentiation and disequilibrium melting lead to the same trace element distribution (see appendix), it could be envisioned that the leucosomes resulted from subsolidus differentiation followed by equilibrium melting of the whole quartzofeldspathic segregations. Nevertheless, it is rather improbable that the subsolidus differentiation of granodioritic gneisses (with a K-feldspar/plagioclase ratio of 0.3) led to quartzofeldspathic segregations characterized by cotectic compositions in the Qtz–Ab–Or system (see for instance Sawyer and Robin 1986).

The near-cotectic composition of the leucosomes suggests that partial melting was the main process of differentiation and controlled the distribution of trace elements between leucosomes and melanosomes. In that case, the trace element patterns of leucosomes and melanosomes are best explained by melting under non-equilibrium conditions and mixing with unmelted residual minerals.

Nevertheless, it should be emphasized that this model is subject to several uncertainties, particularly: (1) the exact mineralogical and chemical composition of the source for each leucosome/melanosome pair is not known, and (2) the solid/solid partition coefficients are approximated from mineral/melt ones.

The fact that the source composition is not accurately known is not a crucial problem. First, uncertainties on the major mineral contents do not have a significant effect on the REE bulk partition coefficient and consequently on the model REE element contents of melts. Second, the calculated difference in REE compositions between both equilibrium and fractional melting models and the disequilibrium one (Fig. 9) is high enough (at least one order of magnitude) to be meaningful despite uncertainties on the trace element abundances in the source rock. Moreover, it appears quite clearly on Fig. 10 that disequilibrium melting is the only model accounting for Rb/Sr ratios in the melts

lower than in the residues. Finally, the Zr content of melt at equilibrium, estimated from Watson's equation, is independant on the Zr content of the source rock but buffered by zircon.

The use of the solid/solid partition coefficients derived from melt/solid ones seems valid. The solid/solid partition coefficients for REE are known for only ultramafic rocks (Stosch 1982). The close agreement between solid/solid partition coefficients estimated from mineral/basaltic melt ones and those published by Stosch suggests that the approximation is valid and can be tentatively applied to felsic melts.

In spite of some uncertainties, the chemical patterns of the leucosomes studied appear to follow the distribution law of the disequilibrium melting model (+mixing with refractory phases). However, is disequilibrium melting a suitable process in crustal anatexis?

The chemical features of partial melts are clearly related to element diffusion between minerals and melts. Consequently, two possible mechanisms can be considered.

(1) The frequent inclusion of these accessories in the major refractory phases (biotite, hornblende) could prevent efficient element diffusion and, therefore, partly account for non-equilibrium melting process. However, the equilibrium Zr content of melt (65–95 ppm) compared to the Zr content of the source rocks (126–274 ppm) shows that saturation can be attained even though ~25% of the total zircon mass is isolated from the melt by inclusion in the major phases. This estimate, consistent with experimental results (Watson and Vicenzi 1988) is significantly higher than observed in the migmatites studied (<1% in the mesosome E114). Therefore, this mechanism cannot account for the behaviour of REE.

(2) The diffusion of trace elements, as for instance Rb, Sr or REE in silicate minerals or melts is a slow process requiring, at the scale of leucosome bodies (5–10 cm), time scales of 10^4–10^6 years (see Hofmann 1980; Tschuiyama 1985). Moreover, bodies of segregated melts in migmatitic terrains are sufficiently small to prevent any convection and therefore efficient element diffusion (see Wickham 1987). On the other hand, melt migration controlled for instance by extensional fracturing can be high enough for a significant segregation to take place over short time spans ($<10^2$ years as discussed by Wickham 1987).

We can reasonably assume that if the melt is segregated from the crystalline residue at a very slow rate, crystals and melt will equilibrate and saturation be reached, leading to equilibrium compositions. On the other hand, if the rate of melt migration is high enough with respect to the rate of element diffusion, melt will not equilibrate with the crystalline residue, leading to disequilibrium melt compositions.

Does this process remain exceptional? Is it restricted to migmatitic terrains or has it a significant bearing on granite genesis at low melt fraction? The answer cannot be given from the present study, but is worth seeking in future.

Conclusion

Zircon U–Pb geochronology clearly indicates the lack of a Kibaran event in the Central Hoggar and suggests that the granodioritic protolith of the Telohat migmatites is Eburnean in age (2.10 Ga) whereas the age of migmatization is around 610 Ma.

Petrologic data and modelling suggest that the chemical patterns of these migmatites, characterized by leucosomes with low Zr and REE contents and near-cotectic compositions, are consistent with partial melting under non-equilibrium conditions. The present study and previous isotopic data raise the question of disequilibrium process in crustal anatexis.

Acknowledgements. Thanks to M. Champenois and A. Kohler for assistance with image processing and S.E.M. respectively. Critical comments by M. Cuney and H. Martin and the thorough and constructive review by an anonymous reviewer are greatfully acknowledged.

Appendix

The following data have been used for trace element modelling during anatexis.

Equilibrium and fractional melting (Allègre and Minster 1978)
Equilibrium melting:

$$C_1 = C_o/[D_o + F(1-P)] \quad (1)$$

Fractional melting + aggregation:

$$C_1 = C_o\,[1-(1-PF/D_o)^{1/P}]/F \quad (2)$$

with

C_o, C_1 = concentration of an element in the initial solid and in the melt respectively

D_o, P = bulk partition coefficients for the initial solid and for the phase assemblage contributing to the liquid

F = degree of melting

See Allègre and Minster (1978) for further details.

Solubility equations for accessory phases (Watson 1987)

The solubility equations used to estimate the equilibrium amount of zircon and apatite dissolved into the melt are respectively:

$$\ln C_{Zr} = 17.18 - 12900/T(\mathrm{K}) \quad (3)$$

$$\ln C_p = 18.08 - 14470/T(\mathrm{K}) \quad (4)$$

The amounts of zircon and apatite are recasted from the Zr and P concentrations in minerals determined by electron microprobe.

Disequilibrium melting

In disequilibrium melting, the melt does not equilibrate with the solid phases and consequently the concentration of an element in the melt depends on its concentration in the minerals of the initial solid and on the mineral proportions which dissolve into the melt (Allègre and Minster 1978):

$$C_1 = \sum C_n \cdot x_n \quad (5)$$

with

C_n = concentration of an element in the mineral(n)
x_n = mass fraction of mineral(n) contributing to the melt

Using partition coefficients between solids, this becomes (Prinzhofer and Allègre 1985):

$$C_1 = C_o\,(M/Q) \quad (6)$$

with

$M = x_1 + D^{2/1} \cdot x_2 + \ldots + D^{n/1} \cdot x_n$
$Q = X_1 + D^{2/1} \cdot X_2 + \ldots + D^{n/1} \cdot X_n$
$D^{2/1}$ = partition coefficient between minerals 2 and 1
x_n = mass fraction of mineral n in the melt
X_n = mass fraction of mineral n in the solid

As the solid/solid partition coefficients are not known, they have been derived from the mineral/melt partition coefficients: $D^{2/1} = D^{2/melt}/D^{1/melt}$. Substituting in Eq. (6), it comes:

$$C_1 = C_o\,(M'/Q') \tag{7}$$

with

$M' = x_1 + (D^{2/m} \cdot x_2 + \ldots + D^{n/m} \cdot x_n)/D^{1/m}$
$Q' = X_1 + (D^{2/m} \cdot X_2 + \ldots + D^{n/m} \cdot X_n)/D^{1/m}$
$D^{2/m}$ = partition coefficient between mineral 2 and melt

The same equation is valid for mixing (mineral entrained into the melt).

Subsolidus differentiation

As no melt phase is involved in subsolidus differentiation, the concentration of an element in a segregation is a direct function of its concentration in the initial minerals and of the weight proportion of minerals entering into the segregation. Therefore, the trace element distribution can be modelled using the same equation as disequilibrium melting.

Partition coefficients

Mineral/melt partition coefficients selected for the calculations are from (1) Arth and Hanson (1976), (2) Martin (1987), (3) Green and Pearson (1986) and (4) Henderson (1982). They are the followings:

	Kfs	Pl	Bt	Grt	Hbl	All	Ap	Sph	Zrn
La	0.08	0.38	0.32	0.39	0.74	960	20	5	4.8
Ce	0.044	0.27	0.32	0.62	1.52	940	34.7	10	4.2
Nd	0.025	0.21	0.29	0.63	4.26	750	57.1	25	3.6
Sm	0.018	0.13	0.26	2.2	7.77	620	62.8	40	4.3
Eu	1.13	2.15	0.24	0.7	5.14	56	30.4	20	3.4
Gd	0.01	0.1	0.28	7.7	10	440	56.3	39	12
Dy	0.006	0.064	0.29	30	13	250	50.7	38	48
Yb	0.012	0.049	0.44	43	8.4	54	23.9	25	280
Rb	0.38	0.09	3.2		0.014				
Sr	5.4	4.5	0.24		0.02				
Ref.	(1)	(1)	(1)	(4)	(1)	(2)	(1)	(3)	(4)

References

Allègre CJ, Minster JF (1978) Quantitative model of trace element behavior in magmatic processes. Earth Planet Sci Lett 38:1–25

Arth JG, Hanson GN (1979) Geochemistry and origin of the early Precambrian crust of northeastern Minnesota. Geochim Cosmochim Acta 39:325–362

Bertrand JML (1974) Evolution polycyclique des gneiss du Précambrien de l'Aleksod (Hoggar Central, Sud algérien). Aspects structuraux, pétrologiques, géochimiques et géochronologiques. Ser Geol CNRS Paris 19:1–350

Bertrand JML, Lasserre M (1976) Pan-African and pre-Pan-African history of the Hoggar (Algerian Sahara) in the light of the new geochronological data from the Aleksod area. Precambrian Res 3:343–362

Bertrand JML, Michard A, Boullier AM, Dautel D (1986) Structure and U–Pb geochronology of Central Hoggar (Algeria): a reappraisal of its Pan-African evolution. Tectonics 5:955–972

Boullier AM, Bertrand JML (1981) Tectonique tangentielle profonde et couloirs mylonitiques dans le Hoggar central polycyclique (Algérie). Bull Soc Geol Fr 23:17–22

Gaby R, Bertrand JML, Black R (1981) Pan-African ocean closure and continental collision in the Hoggar-Iforas segment, Central Sahara. In: A Kröner (ed) Precambrian plate tectonics. Elsevier, Amsterdam, pp 407–434

Carron JP, Lagache M (1980) Etude expérimentale du fractionnement des éléments Rb, Cs, Sr et Ba entre feldspaths alcalins, solutions hydrothermales et liquides silicatés dans le système Q–Ab–Or–H_2O à 2Kbar entre 700 et 800° C. Bull Mineral 103:571–578

Cuney M, Barbey P (1982) Mise en évidence de phénomènes de cristallisation fractionnée dans les migmatites. CR Acad Sci Paris 295:37–42

Deniel C (1985) Apport des isotopes du Sr, du Nd et du Pb à la connaissance de l'âge et de l'origine des leucogranites hymalayens. Exemple du Manaslu (Himalaya, Népal). Thesis, Université de Clermont-Ferrand

Dietrich RV, Mehnert KR (1960) Proposal for the nomenclature of migmatites and associated rocks. Int Geol Congr 21st Copenhagen 1960 Rept Session Norden Suppl Vol Sect 1–21:56–67

Ferry JM, Spear FS (1978) Experimental calibration of the partitioning of Fe and Mg between biotite and garnet. Contrib Mineral Petrol 66:113–117

Flynn RT, Burnham CW (1978) An experimental determination of rare earth partition coefficients between a chloride containing vapor phase and silicate melts. Geochim Cosmochim Acta 42:685–701

Ganguly J, Saxena SK (1984) Mixing properties of aluminosilicate garnets: constraints from natural and experimental data and applications to geothermo-barometry. Am Mineral 69:88–97

Green TH, Pearson NJ (1986) Rare-earth element partitioning between sphene and coexisting silicate liquid at high pressure and temperature. Chem Geol 55:105–119

Gupta LN, Johannes W (1986) Genetic model for the stromatic migmatites of the Rantasalmi-Sulkava Area, Finland. J Petrol 27:521–539

Henderson P (1982) Inorganic geochemistry. Pergamon, Oxford, pp 353

Hodges KV, Spear FS (1982) Geothermometry, geobarometry and the Al_2SiO_5 triple point at Mt. Moosilauke, New Hampshire. Am Mineral 67:1118–1134

Hofman AW (1980) Diffusion in natural silicate melts, a critical review. In: Hargraves RB (ed) Physics of magmatic processes. Princeton University Press, Princeton, pp 385–417

Holdaway MJ (1971) Stability of andalusite and the aluminium silicate phase diagram. Am J Sci 271:97–131

Holtz F, Johannes W, Barbey P, Pichavant M (1988) Liquidus phase relations in the system Qz–Ab–Or at 2 Kbar: the effect of a H_2O. EOS 69:513

Jahn BM, Auvray B, Blais S, Capdevila R, Cornichet J, Vidal P (1980) Trace element geochemistry and petrogenesis of Finnish greenstone belts. J Petrol 21:201–244

Johannes W (1983) On the origin of layered migmatites. In: Ather-

ton MP, Gribble CD (eds) Migmatites, melting and metamorphism. Shiva, Nantwich, pp 234–248
Johannes W, Gupta LN (1982) Origin and evolution of a migmatite. Contrib Mineral Petrol 79:114–123
Kenah C, Hollister LS (1983) Anatexis in the Central Gneiss Complex, British Columbia. In: Atherton MP, Gribble CD (eds) Migmatites, melting and metamorphism, Shiva, Nantwich, pp 142–162
Kretz R (1983) Symbols for rock-forming minerals. Am Mineral 68:277–279
La Roche de H, Leterrier J, Grandclaude P, Marchal M (1980) A classification of volcanic and plutonic rocks using R_1R_2-diagram and major element analyses. Its relationships with current nomenclature. Chem Geol 29:183–210
Latouche L (1978) Le Précambrien de la région des Gour Oumelalen (NE de l'Ahaggar, Algérie). Thesis Université Paris VII, pp 225
Latouche L, Vidal P (1974) Géochronologie du Précambrien de la région des Gour Oumelalen (NE de l'Ahaggar, Algérie). Un exemple de mobilisation du strontium radiogénique. Bull Soc Geol Fr 16:193–203
Lelubre M (1952) Recherches sur la géologie de l'Ahaggar central et occidental (Sahara central). Bull Serv Carte Geol Algérie 22, 2 vols
Martin H (1987) Petrogenesis of Archaean Trondhjemites, tonalites and granodiorites from Eastern Finland: major and trace element geochemistry. J Petrol 28:921–953
Michard A, Albarède F (1986) The REE content of some hydrothermal fluids. Chem Geol 55:51–60
Montel JM (1987) Comportement des terres rares dans les magmas granitiques: modélisation et approche expérimentale du rôle de la monazite. Thesis INPL Nancy, pp 126
Newton RC, Haselton HT (1981) Thermodynamics of garnet-plagioclase-Al_2SiO_5-quartz geobarometer. In: Newton RC, Navrotsky A, Wood BJ (eds). Thermodynamics of minerals and melts. Springer, Berlin Heidelberg, pp 129–145
Pichavant M (1987) Effects of B and H_2O on liquidus phase relations in the haplogranite system at 1 Kbar. Am Mineral 72:1056–1070
Pigage LC, Greenwood HJ (1979) Internally consistent estimates of pressure and temperature: the staurolite problem. Am J Sci 282:943–969
Powell R (1985) Regression diagnostic and robust regression in geothermometer/geobarometer calibration: the garnet-clinopyroxene geothermometer revisited. J Metamorph Geol 3:231–243
Prinzhofer A, Allègre CJ (1985) Residual peridotites and the mechanisms of partial melting. Earth Planet Sci Lett 74:251–265
Pushkar P, Stoeser D (1975) 87Sr/86Sr ratios in some volcanic rocks and some semifused inclusions of the San Francisco volcanic field. Geology 3:669–671
Sautter V (1986) Les éclogites de l'Aleksod (Sud Algérien): des témoins in situ d'une collision continentale. J Afr Earth Sci 5:345–357
Sawyer EW (1987) The role of partial melting and fractional crystallization in determining discordant migmatite leucosome compositions. J Petrol 28:445–473
Sawyer EW, Robin PYF (1986) The subsolidus segregation of layer-parallel quartz-feldspar veins in greenschist to upper amphibolite facies metasediments. J Metamorph Geol 4:237–260
Shaw DM (1970) Trace element fractionation during anatexis. Geochim Cosmochim Acta 34:237–243
Steiner JC, Jahns RH, Luth WC (1975) Crystallization of alkali feldspar and quartz in the haplogranite system $NaAlSi_3O_8-KAlSi_3O_8-SiO_2-H_2O$ at 4 Kb. Geol Soc Am Bull 86:83–98
Stosch HG (1982) Rare earth element partitioning between minerals from anhydrous spinel peridotite xenoliths. Geochim Cosmochim Acta 46:793–798
Thompson AB, Algor JR (1977) Model systems for anatexis of pelitic rocks. I-Theory of melting reactions in the system $KAlO_2$-$NaAlO_2-Al_2O_3-SiO_2-H_2O$. Contrib Mineral Petrol 63:247–269
Tsuchiyama A (1985) Partial melting kinetics of plagioclase-diopside pairs. Contrib Mineral Petrol 91:12–23
Watson EB (1987) The role of accessory minerals in granitoid geochemistry. Hutton Conference on the origin of granites, Edinburgh (Abstr)
Watson EB, Harrison TM (1983) Zircon saturation revisited: temperature and composition effects in a variety of crustal magma types. Earth Planet Sci Lett 64:295–304
Watson EB, Vicenzi EP (1988) Inclusion/Host relations involving accessory minerals in high-grade metamorphic and anatectic rocks. EOS 69:524
Weber C, Barbey P (1986) The role of water, mixing process and metamorphic fabric in the genesis of the Baume migmatites (Ardèche, France). Contrib Mineral Petrol 92:481–491
Weber C, Barbey P, Cuney M, Martin H (1985) Trace element behaviour during migmatization. Evidence for a complex melt-residuum-fluid interaction in the St Malo migmatitic dome (France). Contrib Mineral Petrol 90:52–62
Wickham SM (1987) The segregation and emplacement of granitic magmas. J Geol Soc London 144:281–297
Winkler HGF (1978) Petrogenesis of metamorphic rocks, 5th edn. Springer, New-York Berlin Heidelberg, pp 348

Editorial responsibility: J. Touret
Received May 15, 1988 / Accepted November 28, 1988